



Variable Field Proton–Electron Double-Resonance Imaging: Application to pH mapping of aqueous samples

Valery V. Khramtsov, George L. Caia, Keerthi Shet, Eric Kesselring, Sergey Petryakov, Jay L. Zweier, Alexandre Samouilov*

Davis Heart and Lung Research Institute and the Division of Cardiovascular Medicine, The Ohio State University, College of Medicine, 420 West 12th Ave., Room 611B, Columbus, OH 43210, USA

ARTICLE INFO

Article history:

Received 19 June 2009
Revised 27 August 2009
Available online 26 November 2009

Keywords:

PEDRI, Proton–Electron Double-Resonance Imaging
pH
Functional imaging
DNP, dynamic nuclear polarization,
Nitroxide, spin pH probe

ABSTRACT

A new concept of Variable Field Proton–Electron Double-Resonance Imaging (VF PEDRI) is proposed. This allows for functional mapping using specifically designed paramagnetic probes (e.g. oxygen or pH mapping) with MRI high quality spatial resolution and short acquisition time. Studies performed at 200 G field MRI with phantoms show that a pH map of the sample can be extracted using only two PEDRI images acquired in 140 s at pre-selected EPR excitation fields providing pH resolution of 0.1 pH units and a spatial resolution of 1.25 mm. Note that while concept of functional VF PEDRI was demonstrated using the pH probe, it can be applied for studies of other biologically relevant parameters of the medium such as redox state, concentrations of oxygen or glutathione using specifically designed EPR probes.

Published by Elsevier Inc.

1. Introduction

Broad biomedical applications of nuclear magnetic resonance, NMR and magnetic resonance imaging, MRI, are possible due to the existence of endogenous NMR sensitive nuclei, with concentrations up to 110 M in the case of water protons. MRI has found numerous clinical applications but still suffers from limited functional resolution. On the other hand, electron paramagnetic resonance, EPR, has the unique advantage over NMR in functional specificity due to the absence of overlap with endogenous EPR signals, and has greater sensitivity for the same probe concentration due to the 658 times larger magnetic moment of the electron compared with that of the proton. However, EPR and EPR imaging techniques are far from attaining their maximum potential because of technical limitations which include low depth of penetration of the microwaves in the aqueous sample and short relaxation times of the EPR probes. Since EPR linewidths are 3 orders of magnitude larger than those of NMR, EPRI requires much more powerful gradients [1,2]. Because of the very short electron relaxation times, typically microsecond, pulsed approaches have been limited to paramagnetic probes with long relaxation times [3,4]. Nevertheless, recent advances in pulsed EPR techniques operating at 300 MHz frequency allowed for the first time *in vivo* imaging of

the nitroxide with narrow EPR line [5]. To date, to obtain the highest sensitivity and best quality images, minutes to hours of time are required with common continuous wave (CW) EPR which utilizes stepped gradients. The images obtained give information only on the location of the probe and often lack the anatomic structure required for interpretation [6]. Special efforts are needed to co-register EPRI with anatomic structure [7,8]. Spectral–spatial EPRI is also possible with the CW approach and can provide valuable physiological and functional information [9–14], however even more lengthy acquisition times are required, limiting its applicability, especially for *in vivo* applications.

An alternative imaging modality which also employs unpaired electrons is PEDRI (Proton–Electron Double-Resonance Imaging) [15] or OMRI (Overhauser-enhanced Magnetic Resonance Imaging) [16]. PEDRI as MRI-based technique for *in vivo* imaging of free radicals was first developed in Aberdeen, Scotland, by Dr. D. Lurie and his colleagues [15,17]. Using the PEDRI approach, the EPR signal amplitude spatial distribution is reconstructed from the NMR signal of water protons after irradiation of the paramagnetic solute with an EPR frequency microwave. Under the proper conditions, a transfer of polarization from the electrons to protons occurs by Overhauser effect [18], resulting in enhancement of the NMR signal up to 150 times as measured in biological systems [16,19]. The Overhauser enhancement depends on the RF power, the line width and concentration of the paramagnetic agent, with theoretical maximum enhancement factor of 328. However, practically in

* Corresponding author.

E-mail address: alex.samouilov@osumc.edu (A. Samouilov).

in vivo experiments, considerations of limitation of RF power deposition usually preferred over the maximizing the signal intensity; enhancement of several tens usually preferred for optimal results [20–22].

Recent developments in PEDRI demonstrated that this method allowed simultaneous co-registration of free radical distribution and anatomic information [22,23]. Since PEDRI is based on the proton MRI, it circumvents the resolution limitations of EPRI that occur due to very broad linewidths of most paramagnetic labels, and inherently offers high spatial resolution and rapid image data collection. PEDRI has been used by a few research groups to image free radicals *in vivo* [20,22,24,25] and it is now recognized as a powerful alternative to conventional EPRI. One of the successful applications of functional PEDRI is oxygen mapping. It is based on the paramagnetic character of dissolved oxygen which affects the EPR linewidth of free radical probes and, as a consequence, alters radio frequency power saturability of the probes. Therefore, PEDRI with variable saturation power offers a reliable method of imaging oxygen concentrations *in vivo* using triarylmethyl (TAM) probes [19,20,26,27]. In general, the capacity of PEDRI to reflect EPR spectral properties was demonstrated by distinguishing localizations of ^{14}N and ^{15}N isotope-labeled nitroxides by PEDRI using different EPR irradiation magnetic fields [28].

Previously we applied Field-Cycling DNP (FC DNP) and Field-Cycling PEDRI (FC PEDRI) techniques *in vivo* for obtaining spectral characteristics and spatial distribution of the pH sensitive probe, correspondently [29]. FC DNP approach provided spectral information of the whole sample lacking in spatial resolution. In a complimentary way, FC PEDRI allowed for imaging probe distribution while lacking in spectral information.

In this work, we proposed a new modality of functional imaging in living tissues with enhanced functional and temporal resolution using a PEDRI approach in combination with the original concept of Variable Field (VF) PEDRI. We hypothesized that valuable spectral parameters at each pixel can be extracted from a limited number of PEDRI acquisitions acquired at pre-selected EPR excitation fields. This allows for functional mapping using specifically designed paramagnetic probes (e.g. oxygen or pH mapping) with MRI quality spatial resolution and short acquisition time. The hypothesis has been verified using VF PEDRI and a pH sensitive nitroxide probe. The images were acquired at two pre-selected EPR excitation fields which coincide with EPR spectral peak positions of protonated and nonprotonated forms of the probe. A pH map of the sample was extracted from these two PEDRI images providing pH resolution of 0.1 pH units and a spatial resolution of 1.25 mm. The obtained data shows several fold decrease in acquisition time is possible for VF PEDRI compared with EPRI. This is particularly important for *in vivo* applications where stability of the paramagnetic probes is limited.

2. Materials and methods

2.1. Chemicals

The pH-sensitive nitroxyl radical, 4-amino-2,2,5,5-tetramethyl-3-imidazoline-1-yloxy (R1, Fig. 1) was synthesized as previously described [30].

2.2. FC DNP and FC PEDRI measurements

Field-Cycled (FC) PEDRI images and FC Dynamic Nuclear Polarization (DNP) spectra were obtained using a home-built imager/spectrometer at the Ohio State University [31]. To obtain EPR spectral characteristics, partial cancellation of the detection field B_0^{NMR} is required to alter the evolution field B_0^{EPR} at which the electron

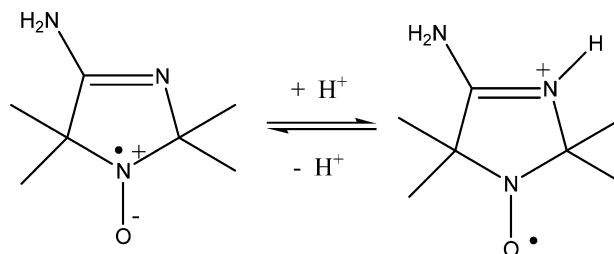


Fig. 1. Protonation of imidazoline pH-sensitive radical, R1. Two main resonance structures are shown illustrating the favored structure with higher unpaired electron density on nitrogen atom N-1 in the nonprotonated form.

paramagnetic resonance (EPR) is excited. This partial cancellation of B_0^{NMR} is achieved by using a secondary electromagnet added to a 0.38 T clinical MRI magnet. The secondary electromagnet built into the gap of the primary magnet provides a vertical magnetic field offset of up to 0.1 T to perform EPR irradiation at the low field followed by high field NMR detection. The field cancellation coils are actively shielded to minimize the effect of eddy currents that occur in the primary magnet. In order to saturate electron spins, a long EPR pulse of relatively high power is needed. For the double-resonance used in PEDRI, a modified Alderman–Grant design resonator with capacitive coupling have been constructed for the EPR excitation channel along with a typical solenoidal coil for the NMR channel [31]. The system is capable of performing fixed-field PEDRI along with two field-cycling modes, FC DNP and FC PEDRI. DNP spectra and images of the phantom samples were collected using field-cycling techniques with an EPR irradiation frequency of 562 MHz (200 G) or 282 MHz (100 G) applied for 500 ms before each collection of a proton signal, and an NMR frequency of 856 kHz (200 G). The repetition time (TR) of the pulse sequence was 1100 ms. The average incident power during an acquisition was 3.3 W. Spectra were obtained by means of a field-cycled DNP pulse sequence in which the evolution field strength was stepped. The EPR irradiation frequency was maintained constant (as was the NMR frequency), so each step of the evolution field was equivalent to the sampling of an EPR signal at a different magnetic field value. The number of steps and their separation defined the overall width of the observed spectrum and its resolution. In this study, spectra of 850 points over a field range of 34 G centered on 200 G (resolution 0.04 G) provided the full three-line spectrum.

2.3. pH titration using FC DNP

The solutions of the R1, 0.5 mM, in water or in 50 mM phosphate buffer were titrated with solutions of HCl or KOH to the required pH, placed in glass tubes of 12 mm diameter for FC DNP spectra acquisition. The observed hyperfine splitting (hfs) measured as the distance between center- and high-field DNP spectral line positions of the triplet has been used as a pH-sensitive parameter. The EPR irradiation field positions that correspond to low- or high-field spectral line positions of fully protonated, RH^+ ($\text{pH} \ll \text{pK}_a$), and fully nonprotonated, R ($\text{pH} \gg \text{pK}_a$), radical forms were measured and used as two pre-selected magnetic fields for pH mapping using VF PEDRI.

2.4. pH mapping using VF PEDRI

The phantom samples were prepared from the glass tubes of 9.5 or 12 mm diameter filled with 0.5 mM solution of the R1 radical in water or in 50 mM phosphate buffer titrated with HCl or KOH to desired pH. This concentration corresponds to administration of 14 μmol of the nitroxide in 28 g mouse, which could be done by bolus i.p. or i.v. injection of 0.4 cc of 35 mM solution. Previously

we have shown that a bolus injection of 0.5 cc of 100 mM nitroxide solution was tolerated by the mice used in the imaging experiments [22].

Field-cycling PEDRI images were collected as 80 mm × 80 mm projective images, with matrices' size of 64 × 64 giving voxel size of 1.25 mm. The field-cycling capability of the system was used to perform EPR irradiation at two pre-selected EPR magnetic fields, $B_{RH^+}^{EPR}$ and B_R^{EPR} corresponding to the peak positions of RH^+ and R forms of the R1 radical, respectively (see Fig. 2). The ratio of NMR signals at each pixel of these two images is pH dependent and was converted to a pH map using a corresponding calibration curve.

3. Results

Fig. 3 shows a typical DNP spectra of the nitroxide R1 ($pK_a = 6.1$ [32]) acquired in acid, pH 4.98, and slightly alkaline, pH 7.62, aqueous solutions corresponding to dominant contributions of the protonated, RH^+ , and nonprotonated, R, forms of the radical, correspondingly. Significantly larger distance between outer lines of the triplet spectra observed for the alkaline solution of the nitroxide is in agreement with previously reported larger nitrogen hyperfine splitting for the R form [32]. Fig. 1 illustrates the effect of protonation of the atom N-3 of the radical heterocycle resulting in decreasing unpaired electron density at the nitrogen of the N–O fragment, and, as consequence, lowered hfs for the RH^+ form. Fig. 4 shows corresponding pH dependent reversible changes of the hfs of the R1 around its $pK_a = 6.1$. Note that at low EPR frequency, 563.2 MHz in Fig. 3, the three lines of the spectrum are unequally spaced due to the Breit–Rabi effect [29,33]. Therefore the hfs values presented in Fig. 4 were measured as the distance between the positions of the center- and high-field spectral lines.

The pH dependent DNP spectral changes allow for preferred excitation of electron paramagnetic resonances of R or RH^+ forms of the nitroxide R1 as illustrated in Fig. 5 for the phantom sample of two tubes filled with the aqueous solution of R1 titrated to alkaline and acidic pHs. The stepped variation of the EPR irradiation field, B^{EPR} , resulted in the subsequent changes in the image intensity with the maximal image intensities of alkaline (predominantly R form) and acidic (predominantly RH^+ form) solutions when B^{EPR} is equal to 83.2 G and 84 G, respectively. Note that the observed 0.8

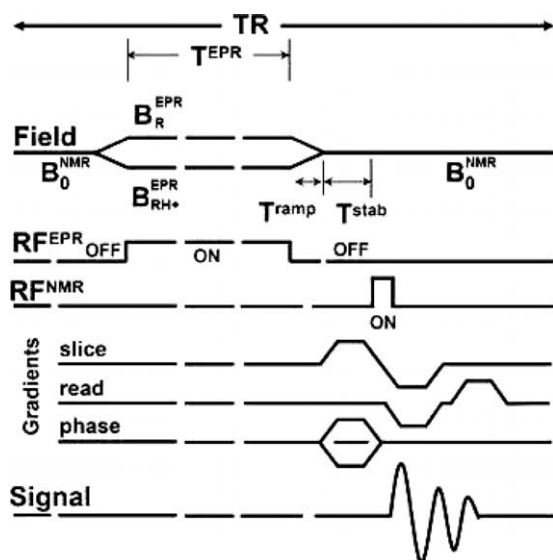


Fig. 2. FC PEDRI pulse sequence with two pre-excitation fields for functional applications.

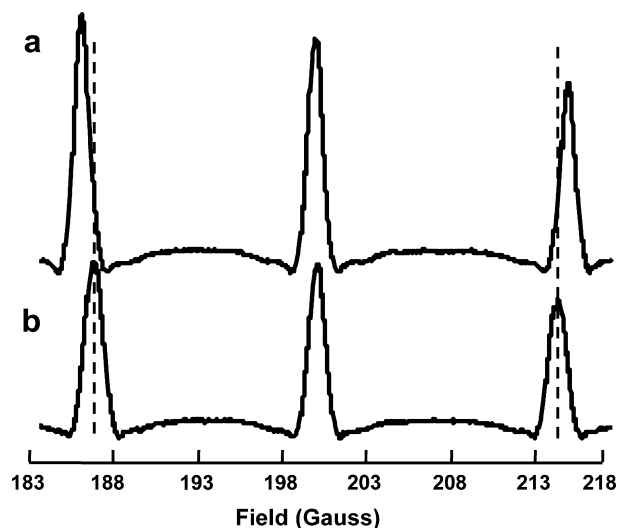


Fig. 3. FC DNP spectra of the nitroxide R1 obtained in phosphate–citrate buffer (10 mM each) at pH 7.62 (a) and pH 4.98 (b). Sample volume was 5 ml. Frequency of EPR irradiation 563.2 MHz, 500 ms, TR 1140 ms; NEX 1; step size = 0.04 G; P = 0.8 W. All other settings were as described in Materials and Methods. A dotted line is extended from low- and high-field peaks of the spectra (b) to aid the eye.

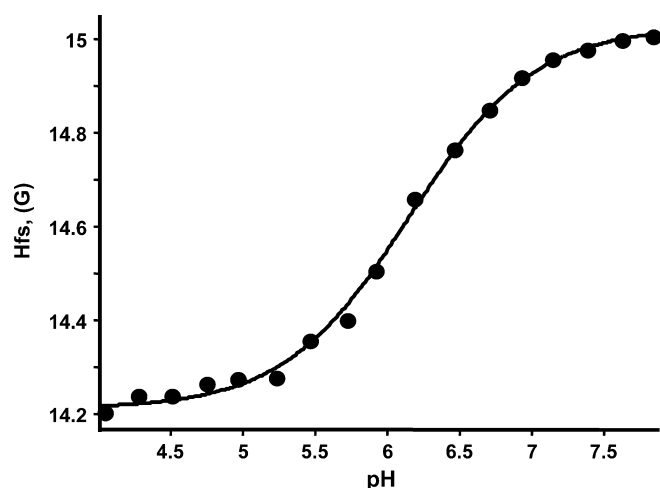


Fig. 4. pH dependence of the hyperfine splitting of the nitroxide R1 measured as the distance between the center- and high-field spectral lines of the DNP spectra. The solid line is a nonlinear least-square fit of the data to a conventional titration curve yielding $hfs(RH^+) = 14.21$ G, $hfs(R) = 15.03$ G and $pK_a = 6.1$.

G difference in B^{EPR} values between the brightest images of R and RH^+ forms is in excellent agreement with maximal pH dependent change of hyperfine splitting shown in Fig. 4.

Based on the data shown in Fig. 5, we hypothesized that in general pH values at each pixel can be extracted from only two PEDRI acquisitions with EPR irradiation at pre-selected EPR fields. Taking into account that the ratio of concentrations of protonated and nonprotonated forms of the probe is directly related to pH ($[RH^+]/[R] = [H^+]/K_a$), we selected the values of EPR excitation fields to coincide with DNP spectral peak positions of RH^+ and R forms of the probe.

Fig. 6 shows pH dependence of the ratio of the corresponding high-field DNP signal amplitudes of RH^+ and R forms of the R1 probe, which allows for ratiometric pH quantification in pH range from 5 to 7. To demonstrate the capacity of VF PEDRI for pH mapping the measurements were performed on the phantom consisting of four tubes, 9.5 mm inner diameter, filled with R1 solution

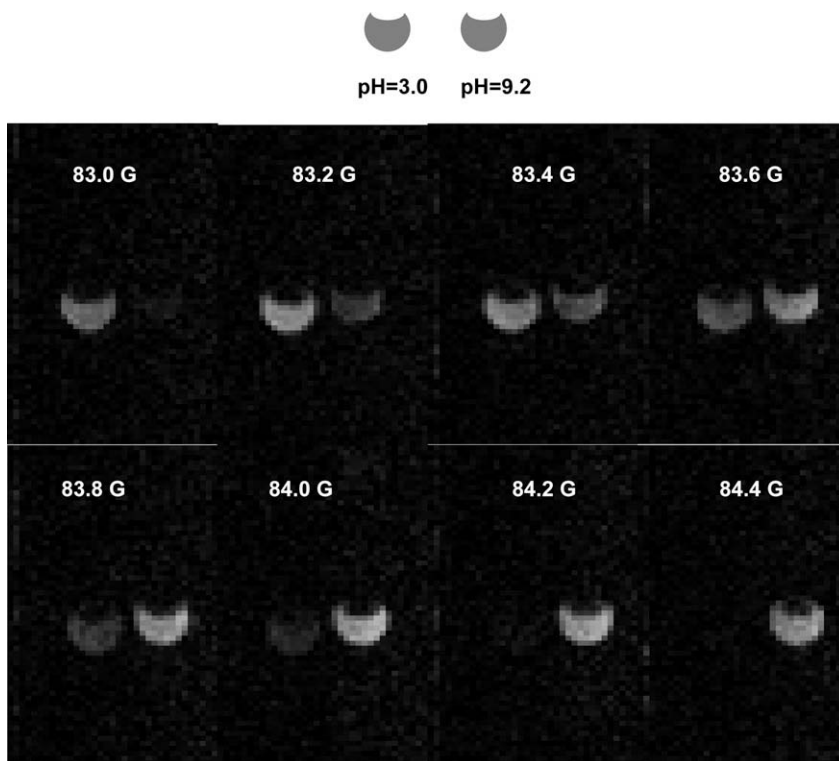


Fig. 5. Sequence of PEDRI images of the phantom sample of a pair of tubes, 12 mm diameter, containing 1 mM aqueous solutions of the R1 probe at pH 9 (left tube) and pH 2 (right tube). Images were acquired at EPR frequency 282 MHz (≈ 100 G for the EPR center field) with evolution field stepped in the range from 83.0 G to 84.4 G around the position of the low-field EPR component of the R1 triplet spectrum. The observed variation of the image intensity with the shift in EPR irradiation field, B^{EPR} (see Fig. 1), illustrates the subsequent changes with the maximal image intensity of R form (left tube) and RH^+ form (right tube) when B^{EPR} is equal to 83.2 G and 84 G, respectively. The PEDRI scan parameters were: TR, 1.1 s; TE, 20 ms; flip angle, 90° ; matrix, 64×64 ; NEX, 1; FOV, 80×80 mm; acquisition time, 70 s.

titrated to different pH values. Fig. 7a shows two PEDRI images of the phantom acquired at EPR frequency 562 MHz (200 G for the EPR center field) and excitation fields, $B_{\text{RH}^+}^{\text{EPR}} = 214.16$ G and $B_{\text{R}}^{\text{EPR}} = 214.88$ G, which correspond to the positions of high-field DNP spectral lines of RH^+ and R forms, respectively.

The ratio of NMR signals at each pixel of these two images (pixel size of 1.25 mm) is pH dependent and was converted to the pH map shown in Fig. 7b using calibration curve. Average pH values

extracted from the image data of the individual tube are in very good agreement with actual pH values. Difference between measured and actual pH does not exceed 0.07. Functional resolution was determined from standard error calculated from the variations of the pH values inside of the individual tube and did not exceed 0.1 U of pH. Spatial resolution of 1.25 mm was calculated as ratio between image field of view and matrix size (64×64).

4. Discussion

The critical role of pH status in physiology and pathophysiology of living organisms is well recognized. At the microscopic level local pH drastically affects the vital activities of the cell, cellular organelles and enzymes. Recently extracellular pH_e has been identified as a significant prognostic factor not only in experimental transplantable tumor models but also in spontaneous tumors [34]. The acidic pH_e in tumors has a number of important consequences, playing a role in tumor initiation, progression, and therapy [35]. Upon therapeutic intervention, the delivery, absorption and pharmacological effectiveness of drugs can be altered by changing the pH of their local environment. Therefore, spatially and temporarily addressed pH measurements *in vivo* are of considerable clinical relevance.

For *in vivo* pH measurements, ^{31}P -NMR has proven to be the most suitable noninvasive approach. However pH assessment using ^{31}P -NMR and inorganic phosphate, P_i has its own limitations, which are rarely discussed, including the lack of resolution (about 0.2–0.3 pH units and even less at lower pH), or the fact that P_i concentrations vary with metabolism and ischemia, and its chemical shift depends on ionic strength [36,37]. Moreover, ^{31}P -NMR using endogenous phosphate reports intracellular pH_i but is practically

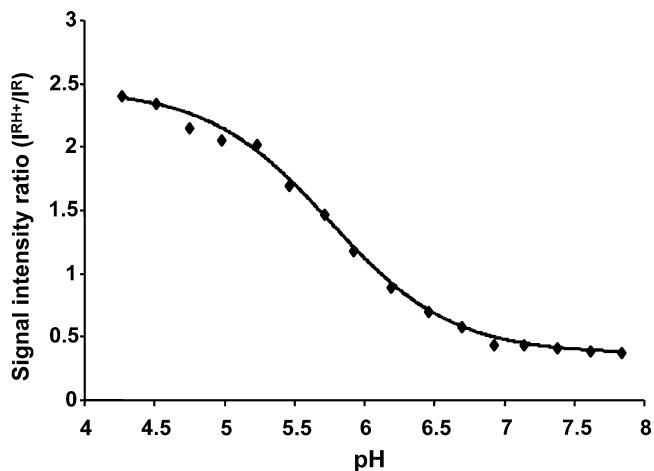


Fig. 6. pH dependence of the ratio of the high-field DNP signal amplitudes measured at EPR excitation field corresponding to maximal intensities of the RH^+ and R forms of the R1 probe. DNP spectra were acquired at EPR frequency 562 MHz (≈ 200 G for the EPR center field), EPR excitation fields were equal to $B_{\text{RH}^+}^{\text{EPR}} = 214.16$ G and $B_{\text{R}}^{\text{EPR}} = 214.88$ G.

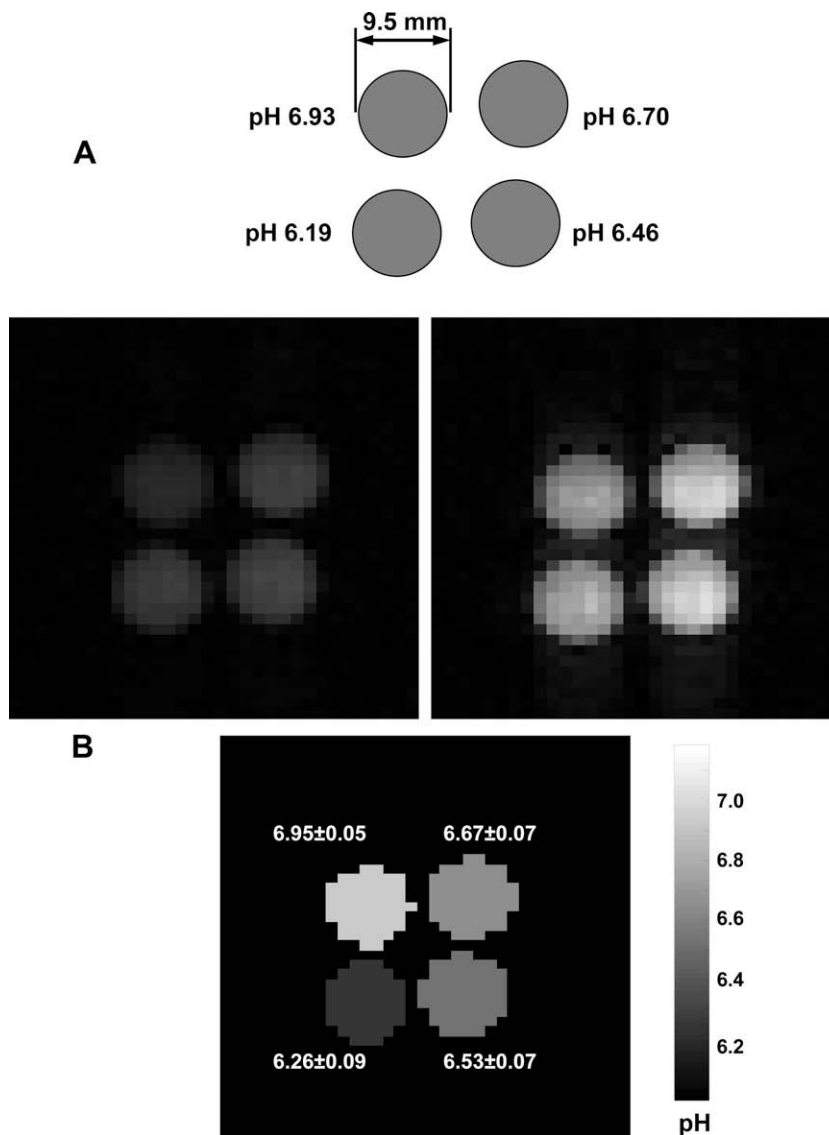


Fig. 7. (A) pH phantom and its PEDRI images acquired at $B_{RH+}^{EPR} = 214.16$ G (left) and $B_{RH+}^{EPR} = 214.88$ G (right). The PEDRI scan parameters were: TR, 1.1 s; TE, 14 ms; flip angle, 90°; matrix, 64×64 ; NEX, 1; FOV, 80×80 mm, acquisition time, 71 s; NMR frequency, 856 kHz. (B) VF PEDRI: proof of concept of functional imaging. pH map of phantom was calculated from two PEDRI images acquired at pre-selected EPR excitation fields as shown in panel (A). Averaged values of pH are given near corresponding tube; functional resolution was determined from standard error calculated from the variations of the pH values inside of the individual tube and did not exceed 0.1 U of pH. Spatial resolution of 1.25 mm was calculated as ratio between image field of view and matrix size (64×64).

insensitive to extracellular pH_e [35]. Therefore several exogenous phosphorus- and fluorine-containing NMR probes were developed for pH measurement using ^{31}P -NMR or ^{19}F -NMR [35].

Application of exogenous probes using EPR spectroscopy has an advantage over exogenous NMR probes in sensitivity and reasonable depth of penetration in living tissues (about 1 cm for commercially available L-band spectrometers). A number of pH sensitive nontoxic nitroxide probes were developed over the last two decades [13,32,38], and have been recently applied to various biological systems, including *in vivo* pH measurements in rodents [29,39,40]. A capacity for pH mapping of aqueous samples using pH sensitive nitroxides and spectral-spatial CW EPRI was also demonstrated for phantom samples [13,41,42]. However the requirement of long acquisition times (typically >1 h for 4D acquisition), high gradients (≥ 30 G/cm), and low spatial resolution make application of CW EPRI for pH mapping of living tissues difficult.

In this work we developed an approach to pH mapping of aqueous samples using pH sensitive nitroxides and VF PEDRI. In general,

PEDRI with variable field EPR pre-excitation allows EPR spectroscopic information to be obtained along with the spatial information on the structure of the object and the distribution of the radical within the object, from the value of the enhancements observed at each pixel. The information obtained is equivalent to that of a 3D or 4D spectral-spatial EPR image along with a superimposed proton MRI. However, complete EPR spectral-spatial reconstruction from VF PEDRI requires multiple MRI acquisitions with a corresponding increase of acquisition time by tens or hundreds fold, making it comparable to 4D spectral-spatial EPRI. Fortunately, valuable spectral parameters at each pixel can be extracted from a limited number of selected PEDRI acquisitions (as little as two) with acquisition time of a few minutes or less. VF PEDRI acquisitions only at two pre-selected EPR excitation fields (70 s each, Fig. 7A) were sufficient to extract pH map with good functional (0.1 pH units) and spatial (1.25 mm) resolutions for the phantom sample with aqueous solutions of pH sensitive nitroxide. An improvement in acquisition time is particularly important for *in vivo* applications where the experimental window and stability

of the nitroxides are limited. Note also that VF PEDRI allows for slice selectivity of the functional image which is unavailable in CW EPRI and possesses the capacity for functional and anatomical resolution in one experimental set-up (otherwise available only in EPR/NMR co-imaging [8]).

In this work the ratiometric approach to mapping pH non-invasively has been demonstrated using a VF PEDRI and pH sensitive nitroxide that has a $pK_a = 6.1$ (Fig. 3). This is useful for pH monitoring in the physiological range or in slightly acidic conditions which are characteristic for ischemic hearts [43] or extracellular tumor microenvironments [35]. A series of pH sensitive nitroxides with enhanced stability against bioreduction and various range of pH sensitivity have been reported and might be used in specific applications [29,44,45]. Moreover, recently the first pH sensitive triaryl-methyl (TAM) radical derivatives which possess an extraordinary stability *in vivo* were developed [46,47]. The amino derivatives of TAM report aqueous acidity in physiological pH range. However, further synthetic efforts are required to develop TAM derivatives based on more hydrophilic structures, such as Oxo63, to improve their aqueous solubility and avoid possible toxicity.

While the concept of functional VF PEDRI was proved using the pH probe, it can be applied for studies of other biologically relevant parameters of the medium such as redox state, concentrations of oxygen or glutathione using specifically designed probes. Recently developed TAM probe with doublet EPR spectrum resulted in enhanced sensitivity to low oxygen concentration [48]. The characteristic oxygen-sensitive EPR field positions corresponding to maximal and minimal peak intensities of the TAM doublet spectrum provide another opportunity for functional (oxygen) mapping using VF PEDRI similar to that for pH with two characteristic pH-sensitive EPR field positions. Recent spectroscopic *in vivo* application of a disulfide biradical probe to report tissue glutathione (GSH) content [49] might also be extended for GSH mapping using VF PEDRI due to the presence of characteristic “biradical” and “monoradical” components in the EPR spectrum.

In this work we employed the FC PEDRI approach with the same NMR detection field (B_0^{NMR}) and EPR evolution field which were only slightly shifted from B_0^{NMR} up or down to fit resonance EPR excitation fields of RH^+ and R forms of the nitroxide. This avoids large field jumps from EPR evolution field to NMR detection field adding stability and decreasing ramping and stabilization times (see Fig. 2). In general, an alternative approach with stationary magnetic field but slightly different EPR radio frequencies can be proposed for functional mapping using specific paramagnetic probes. This approach, which we termed variable radio frequency (VRF) PEDRI, requires minimal instrumental modification of the fixed-field PEDRI system by inclusion of either (i) a wide-band resonator allowing EPR irradiation at close frequencies; or (ii) a dual-frequency switchable resonator. On the other hand, it improves magnetic field homogeneity and stability and decreases acquisition time by eliminating periods of ramping and stabilization of the magnetic field. Moreover, future development of a simplified VRF PEDRI system may allow for elimination of the field-cycling coil and its power supplies, an increased gap in the magnet system, and the possibility to use conventional NMR gradients and gradient power supplies.

5. Conclusion

A new concept of functional mapping using VF PEDRI is proposed and experimentally verified for pH mapping using a pH sensitive nitroxide. The proposed general VF PEDRI approach can be modified for specific studies of other biologically relevant parameters of the medium such as redox state, concentrations of oxygen or glutathione using specifically designed probes.

Acknowledgment

This work was partly supported by NIH grants EB009433, CA132068, EB03519, EB00890 and EB004900.

References

- [1] G.R. Eaton, S.E. Eaton, K. Ohno (Eds.), *EPR Imaging and In vivo EPR*, CRC Press, Boca Raton, 1991.
- [2] P. Kuppusamy, J.L. Zweier, Cardiac applications of EPR imaging, *NMR Biomed.* 17 (2004) 226–239.
- [3] S. Subramanian, M.C. Krishna, Dancing with the electrons: time-domain and CW *in vivo* EPR imaging, *Magn. Reson. Insights* 2 (2008) 43–74.
- [4] K. Matsumoto, S. Subramanian, R. Murugesan, J.B. Mitchell, M.C. Krishna, Spatially resolved biologic information from *in vivo* EPRI, OMRI, and MRI, *Antioxidants Redox Signal.* 9 (2007) 1125–1141.
- [5] F. Hyodo, S. Matsumoto, N. Devasahayam, C. Dharmaraj, S. Subramanian, J.B. Mitchell, M.C. Krishna, Pulsed EPR imaging of nitroxides in mice, *J. Magn. Reson.* 197 (2009) 181–185.
- [6] J.L. Berliner, H. Fujii, Magnetic resonance imaging of biological specimens by electron paramagnetic resonance of nitroxide spin labels, *Science* 227 (1985) 517–519.
- [7] G. He, Y. Deng, H. Li, P. Kuppusamy, J.L. Zweier, EPR/NMR co-imaging for anatomic registration of free-radical images, *Magn. Reson. Med.* 47 (2002) 571–578.
- [8] A. Samouilov, G.L. Caia, E. Kesselring, S. Petryakov, T. Wasowicz, J.L. Zweier, Development of a hybrid EPR/NMR coimaging system, *Magn. Reson. Med.* 58 (2007) 156–166.
- [9] G. He, A. Samouilov, P. Kuppusamy, J.L. Zweier, *In vivo* imaging of free radicals: applications from mouse to man, *Mol. Cell. Biochem.* 234–235 (2002) 359–367.
- [10] S.S. Eaton, M.M. Maltempo, E.D.A. Stemp, G.R. Eaton, 3-Dimensional electron-paramagnetic-res imaging with one spectral and 2 spatial dimensions, *Chem. Phys. Lett.* 142 (1987) 567–569.
- [11] H.J. Halpern, C. Yu, M. Peric, E. Barth, D.J. Grdina, B.A. Teicher, Oxymetry deep in tissues with low-frequency electron paramagnetic resonance, *Proc. Natl. Acad. Sci. USA* 91 (1994) 13047–13051.
- [12] M.C. Krishna, P. Kuppusamy, M. Afeworki, J.L. Zweier, J.A. Cook, S. Subramanian, J.B. Mitchell, Development of functional electron paramagnetic resonance imaging, *Breast Dis.* 10 (1998) 209–220.
- [13] V.V. Khrantsov, Biological imaging and spectroscopy of pH, *Curr. Org. Chem.* 9 (2005) 909–923.
- [14] G. He, A. Samouilov, P. Kuppusamy, J.L. Zweier, *In vivo* EPR imaging of the distribution and metabolism of nitroxide radicals in human skin, *J. Magn. Reson.* 148 (2001) 155–164.
- [15] D.J. Lurie, D.M. Bussell, L.H. Bell, J.R. Mallard, Proton electron double magnetic resonance imaging of free radical solutions, *J. Magn. Reson.* 76 (1988) 366–370.
- [16] K. Golman, I. Leunbach, J.H. Ardenkjaer-Larsen, G.J. Ehnholm, L.G. Wistrand, J.S. Petersson, A. Jarvi, S. Vahasalo, Overhauser-enhanced MR imaging (OMRI), *Acta Radiol.* 39 (1998) 10–17.
- [17] D.J. Lurie, J.M.S. Hutchison, L.H. Bell, I. Nicholson, D.M. Bussell, J.R. Mallard, Field-cycled proton–electron double resonance imaging of free radicals in large aqueous samples, *J. Magn. Reson.* 84 (1989) 431–437.
- [18] A.W. Overhauser, Polarization of nuclei in metals, *Phys. Rev.* 92 (1953) 411–415.
- [19] J.H. Ardenkjaer-Larsen, I. Laursen, I. Leunbach, G. Ehnholm, L.G. Wistrand, J.S. Petersson, K. Golman, EPR and DNP properties of certain novel single electron contrast agents intended for oximetric imaging, *J. Magn. Reson.* 133 (1998) 1–12.
- [20] M.C. Krishna, S. English, K. Yamada, J. Yoo, R. Murugesan, N. Devasahayam, J.A. Cook, K. Golman, J.H. Ardenkjaer-Larsen, S. Subramanian, J.B. Mitchell, Overhauser enhanced magnetic resonance imaging for tumor oximetry: coregistration of tumor anatomy and tissue oxygen concentration, *Proc. Natl. Acad. Sci. USA* 99 (2002) 2216–2221.
- [21] H. Li, Y. Deng, G. He, P. Kuppusamy, D.J. Lurie, J.L. Zweier, Proton electron double resonance imaging of the *in vivo* distribution and clearance of a triaryl methyl radical in mice, *Magn. Reson. Med.* 48 (2002) 530–534.
- [22] H. Li, G. He, Y. Deng, P. Kuppusamy, J.L. Zweier, *In vivo* proton electron double resonance imaging of the distribution and clearance of nitroxide radicals in mice, *Magn. Reson. Med.* 55 (2006) 669–675.
- [23] D.J. Lurie, G.R. Davies, M.A. Foster, J.M. Hutchison, Field-cycled PEDRI imaging of free radicals with detection at 450 mT, *Magn. Reson. Imaging* 23 (2005) 175–181.
- [24] M.A. Foster, I. Seimenis, D.J. Lurie, The application of PEDRI to the study of free radicals *in vivo*, *Phys. Med. Biol.* 43 (1998) 1893–1897.
- [25] H. Utsumi, Molecular imaging of *in-vivo* ROS generation in oxidative diseases using ESRI and OMRI, *Nippon Ronen Igakkai Zasshi* 44 (2007) 11–16.
- [26] D. Grucker, J. Chamberon, Oxygen imaging in perfused hearts by dynamic nuclear polarization, *Magn. Reson. Imaging* 11 (1993) 691–696.
- [27] K. Golman, J.S. Petersson, J.H. Ardenkjaer-Larsen, I. Leunbach, L.G. Wistrand, G. Ehnholm, K.J. Liu, Dynamic *in vivo* oxymetry using overhauser enhanced MR imaging, *J. Magn. Reson. Imaging* 12 (2000) 929–938.

- [28] H. Utsumi, K. Yamada, K. Ichikawa, K. Sakai, Y. Kinoshita, S. Matsumoto, M. Nagai, Simultaneous molecular imaging of redox reactions monitored by overhauser-enhanced MRI with ¹⁴N- and ¹⁵N-labeled nitroxyl radicals, *Proc. Natl. Acad. Sci. USA* 103 (2006) 1463–1468.
- [29] D.I. Potapenko, M.A. Foster, D.J. Lurie, I.A. Kirilyuk, J.M. Hutchison, I.A. Grigor'ev, E.G. Bagryanskaya, V.V. Khrantsov, Real-time monitoring of drug-induced changes in the stomach acidity of living rats using improved pH-sensitive nitroxides and low-field EPR techniques, *J. Magn. Reson.* 182 (2006) 1–11.
- [30] L.B. Volodarsky, I.A. Grigor'ev, Synthesis of heterocyclic nitroxides, in: L.B. Volodarsky (Ed.), *Imidazoline Nitroxides*, CRC Press, Boca Raton, 1988, pp. 5–28.
- [31] S. Petryakov, A. Samouilov, M. Roytenberg, H. Li, J.L. Zweier, Modified Alderman–Grant resonator with high-power stability for proton electron double resonance imaging, *Magn. Reson. Med.* 56 (2006) 654–659.
- [32] V.V. Khrantsov, I.A. Grigor'ev, M.A. Foster, D.J. Lurie, I. Nicholson, Biological applications of spin pH probes, *Cell. Mol. Biol.* 46 (2000) 1361–1374.
- [33] G. Breit, I.I. Rabi, Measurement of nuclear spin, *Phys. Rev.* 38 (1931) 2082–2083.
- [34] M. Lora-Michiels, D. Yu, L. Sanders, J.M. Poulson, C. Azuma, B. Case, Z. Vujaskovic, D.E. Thrall, H.C. Charles, M.W. Dewhirst, Extracellular pH and P-31 magnetic resonance spectroscopic variables are related to outcome in canine soft tissue sarcomas treated with thermoradiotherapy, *Clin. Cancer Res.* 12 (2006) 5733–5740.
- [35] R.J. Gillies, N. Raghunand, M.L. Garcia-Martin, R.A. Gatenby, pH imaging. A review of pH measurement methods and applications in cancers, *IEEE Eng. Med. Biol. Mag.* 23 (2004) 57–64.
- [36] S. Pietri, S. Martel, M. Culcasi, M.C. Delmas-Beauvieux, P. Canioni, J.L. Gallis, Use of diethyl(2-methylpyrrolidin-2-yl)phosphonate as a highly sensitive extra- and intracellular ³¹P NMR pH indicator in isolated organs. Direct NMR evidence of acidic compartments in the ischemic and reperfused rat liver, *J. Biol. Chem.* 276 (2001) 1750–1758.
- [37] R.J. Gillies, J.R. Alger, J.A. den Hollander, R.G. Shulman, Intracellular pH measured by NMR: methods and results, in: R. Nuccitelli, D.W. Deamer (Eds.), *Intracellular pH: its measurement, regulation and utilization in cellular functions*, Alan R. Liss, New York, 1982, pp. 79–104.
- [38] V.V. Khrantsov, L.B. Volodarsky, Use of imidazoline nitroxides in studies of chemical reactions. ESR measurements of the concentration and reactivity of protons, thiols and nitric oxide, in: L.J. Berliner (Ed.), *Spin labeling. The next Millennium*, Plenum Press, New York, 1998, pp. 109–180.
- [39] K. Mader, B. Gallez, K.J. Liu, H.M. Swartz, Non-invasive in vivo characterization of release processes in biodegradable polymers by low-frequency electron paramagnetic resonance spectroscopy, *Biomaterials* 17 (1996) 457–461.
- [40] M.A. Foster, I.A. Grigor'ev, D.J. Lurie, V.V. Khrantsov, S. McCallum, I. Panagiotelis, J.M. Hutchison, A. Koptioug, I. Nicholson, In vivo detection of a pH-sensitive nitroxide in the rat stomach by low-field ESR-based techniques, *Magn. Reson. Med.* 49 (2003) 558–567.
- [41] A. Sotgiu, K. Mader, G. Placidi, S. Colacicchi, C.L. Ursini, M. Alecci, pH-sensitive imaging by low-frequency EPR: a model study for biological applications, *Phys. Med. Biol.* 43 (1998) 1921–1930.
- [42] V.V. Khrantsov, I.A. Grigor'ev, M.A. Foster, D.J. Lurie, J.L. Zweier, P. Kuppusamy, Spin pH and SH probes: enhancing functionality of EPR-based techniques, *Spectroscopy* 18 (2004) 213–225.
- [43] J.L. Zweier, P. Wang, A. Samouilov, P. Kuppusamy, Enzyme-independent formation of nitric oxide in biological tissues, *Nat. Med.* 1 (1995) 804–809.
- [44] I.A. Kirilyuk, A.A. Bobko, I.A. Grigor'ev, V.V. Khrantsov, Synthesis of the tetraethyl substituted pH-sensitive nitroxides of imidazole series with enhanced stability towards reduction, *Org. Biomol. Chem.* 2 (2004) 1025–1030.
- [45] Y.Y. Woldman, S.V. Semenov, A.A. Bobko, I.A. Kirilyuk, J.F. Polienko, M.A. Voinov, E.G. Bagryanskaya, V.V. Khrantsov, Design of liposome-based pH sensitive nanoSPIN probes: nano-sized particles with incorporated nitroxides, *Analyst* 134 (2009) 904–910.
- [46] A.A. Bobko, I. Dhimitruka, J.L. Zweier, V.V. Khrantsov, Trityl radicals as persistent dual function pH and oxygen probes for in vivo electron paramagnetic resonance spectroscopy and imaging: concept and experiment, *J. Am. Chem. Soc.* 129 (2007) 7240–7241.
- [47] I. Dhimitruka, A.A. Bobko, C.M. Hadad, J.L. Zweier, V.V. Khrantsov, Synthesis and characterization of amino derivatives of persistent trityl radicals as dual function pH and oxygen paramagnetic probes, *J. Am. Chem. Soc.* 130 (2008) 10780–10787.
- [48] A.A. Bobko, I. Dhimitruka, T.D. Eubank, C.B. Marsh, J.L. Zweier, V.V. Khrantsov, Synthesis and characterization of trityl-based EPR probe with enhanced sensitivity to oxygen, *Free Rad. Biol. Med.* 47 (2009) 654–658.
- [49] G.I. Roshchupkina, A.A. Bobko, A. Bratasz, V.A. Reznikov, P. Kuppusamy, V.V. Khrantsov, In vivo EPR measurement of glutathione in tumor-bearing mice using improved disulfide biradical probe, *Free Rad. Biol. Med.* 45 (2008) 312–320.